Vol. 18, No. 1 (2019) 349-360
Revista Mexicana de Ingeniería Química

SIMULATION AND CONTROL OF REACTANTS SUPPLY AND REGULATION OF AIR TEMPERATURE IN A PEM FUEL CELLS SYSTEM WITH CAPACITY OF 50 KW

SIMULACIÓN Y CONTROL DEL SUMINISTRO DE REACTANTES Y REGULACIÓN DE LA TEMPERATURA DEL AIRE EN UN SISTEMA DE CELDAS DE COMBUSTIBLE TIPO PEM CON CAPACIDAD DE 50 KW

A. Cruz-Rojas[1], J.Y. Rumbo-Morales[1]*, J. de la Cruz-Soto [3], J.A. Brizuela-Mendoza[4], F.D.J. Sorcia-Vázquez[4], M. Martínez-García[4]

[1]*Tecnológico Nacional de México, TecNM/CENIDET, Int. Internado Palmia S/N, Col. Palmira, Cuernavaca C.P. 62490, Mexico.*
[2]*Universidad Tecnologica Emiliano Zapata. Av. Universidad Tecnológica, C.P. 62760, Emiliano Zapata, Morelos.*
[3]*CONACYT-INEEL. Av. Reforma 113, Palmira, C.P. 62490 Cuernavaca, Morelos.*
[4]*Universidad de Guadalajara. Centro Universitario de los Valles. Carretera Guadalajara-Ameca Km. 45.5 C.P. 46600, Ameca, Jalisco, México.*

Received: July 18, 2018; Accepted: September 11, 2018

Abstract

Nonlinear models of both a heat exchanger for cathode and a direct current electric motor to drive the compressor are sized and incorporated to the mathematical model of a PEM fuel cell system with capacity of 50 kW of net power intended to propel an electric vehicle. A balance of plant is achieved through several controllers to the main control loops. A Model Reference Adaptive Controller is used to regulate the oxygen excess ratio manipulating the voltage applied to the electric motor. Proportional-Integral controllers are designed to regulate the air temperature entering to the cathode and to minimize the pressure difference between the cathode and anode. Despite the non-minimum phase behavior observed in the net power delivered by the stack, the closed-loop system tolerates changes in current demand and keeps the compressor operating in its region of maximum efficiency.

Keywords: PEM fuel cell, MRAC, heat exchanger, oxygen excess ratio.

Resumen

Se incorporan y dimensionan los modelos no lineales tanto de un intercambiador de calor para el cátodo como el de un motor eléctrico de corriente directa para impulsar el compresor al modelo matemático no lineal de un sistema de celdas de combustible tipo PEM con capacidad de 50 kW de potencia neta destinado para propulsar un vehículo eléctrico. Se realiza un balance de planta a través del uso de varios controladores en los lazos principales. Se usa un controlador adaptable con modelo de referencia para regular la relación de exceso de oxígeno manipulando el voltaje aplicado al motor eléctrico. Se diseñan controladores tipo Proporcional-Integral-Derivativo tanto para regular la temperatura del aire que entra al cátodo como para minimizar la diferencia de presión entre el cátodo y el ánodo. A pesar del comportamiento de fase no mínima que se observa en la potencia neta que entrega el apilamiento el sistema en lazo cerrado tolera cambios en la demanda de corriente y mantiene al compresor operando en su región de máxima eficiencia.

Palabras clave: Celda de combustible PEM, MRAC, intercambiador de calor, relación de exceso de oxígeno.

1 Introduction

Fuel cells are electrochemical devices that convert the chemical energy of a fuel into electricity and are considered as alternative energy sources for both mobile and stationary applications.

At the moment the systems of feeding based on Proton Exchange Membrane Fuel Cell (PEMFC) are taking major importance due to the necessity to improve the environmental conditions, but mainly due to the depletion of the petroleum (Barelli *et al.*, 2011,

* *Corresponding author. E-mail*: jjrumbo@hotmail.com
doi: https://doi.org/10.24275/uam/izt/dcbi/revmexingquim/2019v18n1/Martinez
issn-e: 2395-8472

Pérez-Rodriguez *et al.*, 2018 and Téllez-Méndez *et al.*, 2018). The industry of electric vehicles, in order to enter the market, is already selling cars fed by fuel cells (Hwang *et al.*, 2012). However, in most cases, their designs omit many contributions that have been made in this area, so that vehicles can be improved (H.-W. Wu, 2016).

The mathematical model published by Pukrushpan *et al.* (2004) and Pukrushpan *et al.* (2002) is the most widely used to simulate fuel cell systems, however, the author omits the heat exchanger needed to reduce the air temperature, besides, the electric motor driving the compressor is poorly described.

Particularly, terminals of the stack must be connected to the field winding of the electric motor, so the variations in voltage of these terminals represent disturbances for the motor. Shuang Zhai *et al.* (2010) present a simulation platform for power systems based on PEM fuel cells, the stacking is simulated by a distributed parameter model and auxiliary units based on concentrated parameter models. The results show that the overshoot in the output voltage is due to the delays in the responses of the auxiliary units.

Gerard *et al.* (2012) propose a new analysis in the degradation of the performance of a PEMFC system during the lack of oxygen, carried out durability tests in the stack and found oscillations in the voltage.

Ye *et al.* (2009) simulated in Aspen Plus the production of hydrogen by reforming methane vapor. To simulate the process they used the sub-model of the minimum free energy of Gibbs and for the humidification of hydrogen they integrated a sub-routine FORTRAN in Aspen Plus. Fuel cells are known as devices with slow response and unable to deliver high rates of power. NikiforowJ *et al.* (2017) show how to an air supply strategy can lead the fuel cell to provide a significant amount of power in less than 1 second.

Humidification in a PEMFC has a strong impact on cell performance (Aleksandra Sveshnikova *et al.*, 2017). The author shows how to an increase in humidification temperature produces an increase in cell voltage, no matter the current density range.

Abid Rabbani *et al.* (2017) developed a model to be used for optimized and design operational strategies for PEMFC systems for automotive applications. The model incorporates thermal behavior, water crossover, mass, and energy balances.

Hosseinzadeh *et al.* (2013) contributed significantly addressing the balance of plant of a fuel cell system. In the analysis, all auxiliary equipment addressed here except the electric motor are included, besides, the controllers that allow changes in the current demand are not included. To construct the simulator of the fuel cell system, part of the mathematical models contributed by Pukrushpan (2003) were used, as well as the procedures that are reported in the articles to work with Aspen Plus.

In this work, both a heat exchanger and an electric motor are sized under air flow requirements and then they are incorporated to the fuel cell system. the mathematical model of the complete system results with 13 state variables, which allows to have a greater precision of its dynamics and at the same time allows to improve the design of the controllers. The balance of plant is achieved by including controllers for the main three control loops of the system.

After addressing the work related to the fuel cell system in section 1, in section 2 the dynamic model of the complete fuel cell system is presented. This section is divided into three parts: in section 2.1 the mathematical models of the cathode, the anode and the manifold that make up the fuel cell are shown; in section 2.2 the direct current electric motor model is presented and its sizing is performed; and in section 2.3 the model of the heat exchanger for the cathode is presented and its sizing is also included. In section 3 the controllers for the three main control loops of the system are designed. And finally, in section 4 the dynamic analysis that was obtained when the system in closed loop is simulated is shown.

2 Materials and methods

2.1 Mathematical model of the PEM fuel cell system

During the operation of the PEM fuel cell, two chemical reactions occur, one at the anode and one at the cathode. At the anode the fuel undergoes oxidation reactions that generate protons (hydrogen ions with positive charge) and electrons. After the oxidation reaction the protons flow from the anode to the cathode through the polymer membrane; at the same time the electrons flow in the same direction but through an external circuit thus producing a direct current. At the cathode, hydrogen ions react with electrons and oxygen to form water (Pukrushpan *et al.*, 2004; Schefflan *et al.*, 2011; Bequette, 1998; Maya-Yescas *et al.*, 2006).

2.1.1 *Dynamic model of cathode, anode, and manifolds.*

Since air is a mixture of nitrogen and oxygen, the mass balance must be made for both as well as for the accumulated water, which is described in equations (1)-(2)-(3); similarly, at the anode, the mass balance is made for hydrogen and for the accumulated water, which is described in equations (4)-(5).

The air conditions change after going through the compressor, the heat exchanger and the humidifier, so it is necessary to know its mass, its outlet pressure and its return pressure, as indicated by equations (6)-(7) and (8). The relation $\lambda_{O_2} = W_{O_2ca,in}/W_{O_2,reacted}$ is known as oxygen excess ratio.

$$\frac{dm_{O_2ca}}{dt} = W_{O_2ca,in} - W_{O_2ca,out} - W_{O_2,reacted} \quad (1)$$

$$\frac{dm_{N_2ca}}{dt} = W_{N_2ca,in} - W_{N_2ca,out} \quad (2)$$

$$\frac{dm_{\omega,ca}}{dt} = W_{v,ca,in} - W_{v,ca,out} + W_{v,ca,gen} + W_{v,membr} - W_{l,ca,out} \quad (3)$$

$$\frac{dm_{H_2,an}}{dt} = W_{H_2an,in} - W_{H_2an,out} - W_{H_2,reacted} \quad (4)$$

$$\frac{dm_{\omega,an}}{dt} = W_{v,an,in} - W_{v,an,out} - W_{v,membr} - W_{l,an,out} \quad (5)$$

$$\frac{dm_{sm}}{dt} = W_{cp} - W_{sm,out} \quad (6)$$

$$\frac{dp_{sm}}{dt} = \frac{\gamma R_a}{V_{sm}}(W_{cp}T_{cp,out} - W_{sm,out}T_{sm}) \quad (7)$$

$$\frac{dp_{rm}}{dt} = \frac{R_a T_{rm}}{V_{rm}}(W_{ca,out} - W_{rm,out}) \quad (8)$$

There are additional algebraic equations describing other variables of the fuel cell. The voltage at the terminals of the stack is calculated using (9), and the output net power is calculated using (10).

$$v_{st} = n(E - v_{act} - v_{ohm} - v_{conc}) \quad (9)$$

here E is the open circuit voltage, v_{act} is the voltage due to activation losses, v_{ohm} is the voltage due to ohmic losses, v_{conc} is the voltage due to concentration losses and n is the number of mono-fuel cells; all of them are found in Pukrushpan *et al.* (2004).

The power produced by the stack is calculated as the product of the voltage at its terminals (v_{st}) and the current demanded by the charge (I_{st}). Note that to calculate the net power (P_{net}) only the power consumed by the electric motor of the compressor ($P_{cm,in}$) is deducted since this constitutes the main parasitic power.

$$P_{net} = v_{st}I_{st} - P_{cm,in} \quad (10)$$

2.1.2 *Sizing of the electric motor that drives the compressor*

The compressor considered to supply the air to the fuel cell is driven by a direct current electric motor. To simulate it, the nonlinear model proposed by Khalil *et al.* (1996) is used. Equations (11)-(12)-(13) describe the dynamic behavior of the electric motor by three state variables (Ljung, 1999; Luyben, 2002).

$$\frac{di_a}{dt} = \frac{v_{st} - R_f i_f}{L_f} \quad (11)$$

$$\frac{di_f}{dt} = \frac{v_{cm} - c_1 i_f \omega_{cp} - R_a i_a}{L_a} \quad (12)$$

$$\frac{d\omega_{cp}}{dt} = \frac{\tau_{cm} - \tau_{cp}}{J_{cp}} \quad (13)$$

The mathematical model indicates that the field winding and the armature winding are fed independently. The variable v_{st} is the voltage supplied to the field winding, and it comes from the terminals of the fuel cell stack, while v_{cm} is the voltage that feeds the armature winding. This voltage must be obtained from a DC-DC converter which is not simulated here.

The state variables of the sub-model are the followings: i_a is the current of the armature, i_f is the field current, and ω_{cp} is the angular velocity of the motor. On the other hand, as parameters of this sub-model are the following: R_f and L_f are the resistance and inductance of the field winding, R_a and L_a are the resistance and the inductance of the armature; and the moment of inertia of the compressor is denoted as J_{cp}.

The term τ_{cm} represents the torque produced by the electric motor and it can be calculated by using the equation (14). At first, τ_{cp} is calculated by using the equation (15) but later it will be replaced by the coupled actual load.

$$\tau_{cm} = c_2 i_f i_a \quad (14)$$

$$\tau_{cp} = c_3 \omega_{cp} \tag{15}$$

The power consumed and supplied by the electric motor is calculated using (16)-(17), respectively.The efficiency which electric energy is converted to mechanical energy η_{cp} is calculated using (18).

$$P_{cm,in} = v_{st} i_f + v_{cm} i_a \tag{16}$$

$$P_{cm,out} = \omega_{cp} \tau_{cp} = c_3 \omega_{cp}^2 \tag{17}$$

$$\eta_{cm} = \frac{P_{cm,out}}{P_{cm,in}} \tag{18}$$

The numerical value of the parameters c_1, c_2, c_3, R_f, i_a, and i_f is obtained by solving the following system of algebraic equations simultaneously.

$$c_3 = \frac{\bar{\tau}_{cp}}{\bar{\omega}_{cp}} \tag{19}$$

$$\eta_{cm} = \frac{c_3 \bar{\omega}_{cp}^2}{\bar{v}_{st} i_f + \bar{v}_{cm} i_a} \tag{20}$$

$$c_2 i_f i_a = \bar{\tau}_{cm} \tag{21}$$

$$i_a = k\, i_f \tag{22}$$

$$R_f = \frac{\bar{v}_{st}}{i_f} \tag{23}$$

$$c_1 = \frac{\bar{v}_{cm} - R_a i_a}{i_f \bar{\omega}_{cp}} \tag{24}$$

The coefficient k in the equation (22) only indicates the number of times armature current exceeds field current and it depends on the designer.

For the sizing of the electric motor it was necessary to use the nominal values of some variables of the fuel cell system that it simulated (Pukrushpan *et al.*, 2004). These values were obtained when the demanded current is 280 A and are presented in Table 1.

Parameters J_{cp} and η_{cm} were also taken from (Pukrushpan *et al.* 2004); parameters R_a, L_a, L_f, and $\bar{v}_{cm}$ were simply proposed with appropriate values. All motor parameters with their values are shown in Table 1.

Now, equation (15) which calculate the actual torque consumed by compressor can be replaced by (25).

$$\tau_{cp} = \frac{c_{p,air}}{\omega_{cp}} \frac{T_{atm}}{\eta_{cp}} [(\frac{p_{sm}}{p_{atm}})^{\frac{\gamma-1}{\gamma}} - 1] W_{cp} \tag{25}$$

Table 1. Parameters for the electric motor model.

c_1	1.30×10^{-3}
c_2	3.93×10^{-3}
c_3	1×10^{-5}
R_a	5.99 c
R_f	30.10 Ω
i_a	15.94 A
i_f	7.97 A
$\bar{\omega}_{cp}$	1×10^4 rad/s
L_a	500 mH
L_f	500 mH
J_{cp}	5×10^{-5} $kg\ m^2$
$\bar{v}_{st}$	240.0 $volts$
$\bar{v}_{cm}$	200.0 $volts$
$\bar{\tau}_{cp}$	0.5 Nm
$\bar{\tau}_{cm}$	0.5 Nm
η_{cm}	0.98
k	2.0

2.1.3 Sizing of heat exchanger for cathode

Pukrushpan *et al.* (2004) provides an equation to calculate the temperature at which the air leaves the compressor (26). In this equation T_{atm} and p_{atm} are the atmospheric air temperature and pressure, respectively, p_{sm} is the air pressure at the compressor outlet, η_{cp} is the efficiency of the compressor and $\gamma = 1.4$ is the ratio of specific heats for air. When simulating this equation, it is found that the maximum temperature at which the air leaves the compressor is $446K$; if the air enters the cell under these conditions, the polymer membrane will be damaged, so this temperature value must be reduced to $353K$, which is the maximum temperature value that the membrane supports. The value of $446K$ is used in this section to design the heat exchanger for the cathode.

$$T_{cp,out} = T_{atm} + \frac{T_{atm}}{\eta_{cp}} \left[\left(\frac{p_{sm}}{p_{atm}} \right)^{\frac{\gamma-1}{\gamma}} - 1 \right] \tag{26}$$

To reduce the air temperature a heat exchanger of concentric tubes is used. To simulate this heat exchanger a simplified nonlinear mathematical model

of stirred tank heat exchanger described by the equations (27)-(28) is employed (Astorga *et al.*, 2008).

$$\frac{dT_{ca,in}}{dt} = \frac{W_{cp}}{V_{sm}\rho_a}(T_{cp,out} - T_{ca,in}) - \frac{UA}{c_{p,a}V_{sm}\rho_a}(T_{ca,in} - T_{\omega}) \tag{27}$$

$$\frac{dT_{\omega}}{dt} = \frac{W_{\omega}}{V_{\omega}\rho_{\omega}}(T_{cold} - T_{\omega}) - \frac{UA}{c_{p,\omega}V_{\omega}\rho_{\omega}}(T_{\omega} - T_{ca,in}) \tag{28}$$

It can be seen that many of the parameters used in the heat exchanger model correspond to those of the fuel cell system, such as the compressor mass flow W_{cp}, the air temperature $T_{cp,out}$, and the supply manifold volume V_{sm}.

The use of a refrigerator to reduce the air temperature constitute another parasitic power, therefore a radiator is preferred. This radiator must maintain the temperature of the cooling fluid to 298 K, which is the ambient temperature for tropical climates.

Parameters as the product UA and the cooling water flow W_{ω} were calculated from mathematical model of the heat exchanger at steady state, i.e. making equations (27)-(28) zero, while the load demanded was 280 A. Particularly, the heat transfer area A was obtained simulating a HEATER block in Aspen Plus using the flow and temperature requirements. The parameters are shown in Table 2.

2.2 *Design of controllers for PEM fuel cell system*

A change in the current demanded by load implies a consequent change in the flow of the reactants; the oxygen flow is the first thing to change because the dynamics in the supply of oxygen is slower than that of hydrogen. While hydrogen is supplied manipulating a valve, oxygen must be taken from the atmosphere using a compressor driven by a direct current electric motor (Rubio *et al.*, 2012; Gómez *et al.*, 2017; Cantero *et al.*, 2017; Rumbo-Morales *et al.*, 2018).

The variation in the flow of the reactants results in the variation of pressure. Since the polymer membrane that separates the cathode and the anode has a low mechanical strength (Javier de la Cruz *et al.*, 2018 and Javier de la Cruz *et al.*, 2016) it is necessary to minimize the pressures difference between both electrodes, otherwise, the membrane would break. Therefore, the regulation of the pressure at the anode p_{an} is needed by manipulating the hydrogen flow $W_{an,in}$ and using pressure at the cathode p_{ca} as setpoint. To perform this task, a PI controller described with equations (29)-(30) is used.

Table 2. Design parameters used to simulate the Heat Exchanger model.

Hot fluid (air)	
$\bar{W}_{cp}$	0.076 kg/s
$\bar{T}_{cp,out}$	432.79 K
$\bar{T}_{ca,in}$	353.15 K
Cooling fluid (water)	
$\bar{W}_{\omega}$	3.128×10^{-2} kg/s
T_{cold}	298.15 K
$\bar{T}_{\omega}$	345 K
General parameters	
U	3106.45 W/m^2K
A	0.2419 m^2
V_{ω}	2.46×10^{-5} m^3

This controller was tuned by using pole placement method and its gains are shown in Table 3.

$$e_1 = p_{ca} - p_{an} \tag{29}$$

$$W_{an,in} = k_{p1}e_1 + k_{i1}\int e_1 dt \tag{30}$$

The oxygen excess ratio ($\lambda_{O_2} = W_{O_2ca,in}/W_{O_2,reacted}$) indicates the proportion in which the fuels are consumed. According to Pukrushpan *et al.* (2004) its value must be 2; if this is the case, a total fuel consumption is guaranteed and consequently an operation in the region of maximum power of the system is also guaranteed; therefore, this ratio is the most important variable of the complete system.

Regulation of the oxygen excess ratio is done by manipulating the voltage supplied to the electric motor v_{cm} driving the compressor. Changes in the current demanded by load I_{st} together with variations in the voltage delivered by stack v_{st} are its main disturbances. A Model Reference Adaptive Controller (MRAC) was used in this control loop (Åström *et al.*, 2013; Åström *et al.*, 1988). Since this controller operates in regulation mode, shaded elements in the controller block diagram (Fig.) were not needed. The gain of the adaptive controller σ was the unique found heuristically.; besides parameter a_m can take any positive real value.

Table 3. Controllers for each loop with their respective gains.

Loop variable		Controller	Gains
Manipulated	Regulated		
v_{cm}	λ_{O_2}	MRAC	$\sigma = 145$
$W_{an,in}$	p_{an}	PI1	$k_{p1} = 10^{-4}, k_{i1} = 10^{-3}$
W_{ω}	$T_{ca,in}$	PI2	$k_{p2} = -0.5, k_{i2} = -2.0$

An air temperature $T_{ca,in}$ exceeding 353.15 K also hurt the polymer membrane. Incorporation of a heat exchanger allows regulation of this variable manipulating the cooling water flow W_{ω}. To perform this task, a PI controller described with equations (33)-(34) is used. In order to be able to tune the PI controllers it was necessary to linearize the system at one point of operation. This linearization was done using input and output data of both the manipulated variable and the variable to be controlled. To identify the temperature of the air at the outlet of the cathode, the mass flow of the cooling fluid was manipulated; to identify the pressure at the anode, the mass flow of hydrogen was manipulated. In both cases, an PRBS was introduced and the identification tool that was used was "output error".

$$\frac{p_{an}(s)}{W_{an,in}(s)} = \frac{3.364 \times 10^6}{s + 8.032} \tag{31}$$

$$\frac{T_{ca,in}(s)}{W_{\omega}(s)} = \frac{-7847}{s + 3.285} \tag{32}$$

The transfer functions were first grade, described with equations (31)-(32), so a PI controller was sufficient to perform the control over the entire operating range. Once the transfer functions were obtained, the pole positioning method was applied to establish the dynamics of each variable in a closed loop, which provided them with a unit gain. The poles were established with a faster dynamic than in open loop and always in the left half plane to confer stability to the system.

$$e_2 = 353.15 - T_{air} \tag{33}$$

$$W_{\omega} = k_{p2} e_2 + k_{i2} \int e_2 dt \tag{34}$$

Table 3 presents the parameters of the controllers in a synthesized manner. The Fig. 2 shows a process diagram that shows the complete system with its control loops. The initial conditions for all system variables are presented in Table 4.

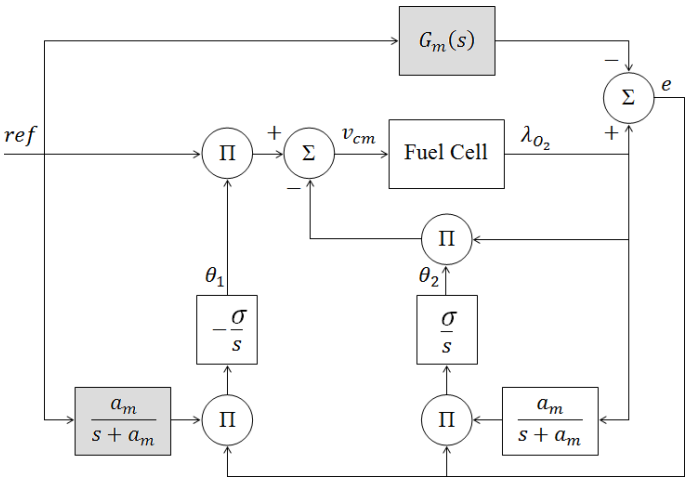

Fig. 1. MRAC controller block diagram for regulating oxygen excess ratio.

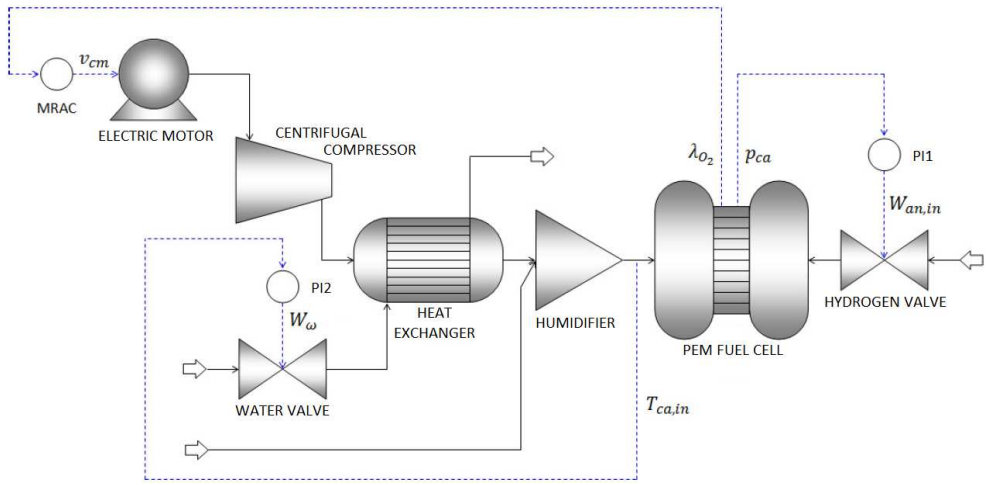

Fig. 2. Process diagram flowsheet for the PEM fuel cell system with their respective control loops.

Table 4. Initial conditions used to simulate the PEM fuel System.

Cathode
$m_{O_2,ca}(0) = 1.289 \times 10^{-3}\ kg$
$m_{N_2,ca}(0) = 8.489 \times 10^{-3}\ kg$
$m_{\omega,ca}(0) = 12.95\ kg$
Anode
$m_{H_2,an}(0) = 3.46 \times 10^{-4}\ kg$
$m_{\omega,an}(0) = 6.594\ kg$
Supply Manifold
$m_{sm}(0) = 3.067 \times 10^{-2}\ kg$
$p_{sm}(0) = 1.517 \times 10^{5}\ Pa$
Return Manifold
$p_{sm}(0) = 1.281 \times 10^{5}\ Pa$
Direct Current Electric Motor
$i_f(0) = 8.174\ A$
$i_a(0) = 7.839\ A$
$\omega_{cp}(0) = 5.605 \times 10^{3}\ rad/s$
Heat Exchanger
$T_{ca,in}(0) = 353.15\ K$
$T_\omega(0) = 353.48\ K$
Integrators
$I_{\theta_1}(0) = -7.095$
$I_{\theta_2}(0) = 6.726$
$I_1(0) = 16.91$
$I_2(0) = 5.37 \times 10^{-4}$
Load Current Demand
$I_{st}(0) = 110\ A$

3 Results and discussion

After incorporate the heat exchanger for the cathode and the direct current electric motor, the mathematical model for the complete system of PEM fuel cell was left with thirteen state variables.

The adaptive controller is able to regulate the ratio of excess oxygen to a value of two having oscillations during the transient periods, as indicated in the Fig. 3. Note that v_{cm} is the control signal thrown by the adaptive controller and applied directly to the armature winding of the electric motor. With higher gains, the electric motor would receive signals of greater magnitude and its performance would be detrimental. For comparative purposes, the current demand used here is the same as that used by Pukrushpan *et al.* (2004).

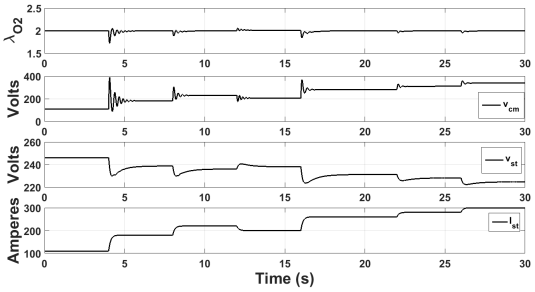

Fig. 3. Oxygen excess ratio λ_{O_2}, voltage supplied to the compressor v_{cm}, voltage produced by the stack v_{st}, and current demanded by load I_{st}, respectively.

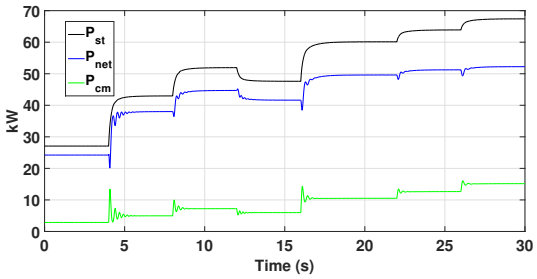

Fig. 4. Total power produced by the system P_{st}, net power delivered by the system P_{net}, and parasitic power consumed by the motor coupled to the compressor $P_{cm,in}$.

The net power (P_{net}) delivered by the system reaches a maximum value of 52 kW as indicated in the Fig. 4. Based on (Pukrushpan *et al.*, 2004), this power is sufficient for a four-seater vehicle. It can also be seen that, for each change in the point of operation, the net power has a downward overshoot. This overshoot is caused by the power peak consumed by the electric motor of the compressor ($P_{cm,in}$), whose energy is taken from the energy produced by the fuel cell itself. This new effect makes the plant a non-minimum phase system.

By zooming the voltage produced by the stacking a small ripple can be observed (probably due to a reduction of ohmic losses), as shown in the Fig. 5. This ripple occurs only when the heat exchanger for the cathode is incorporated and its amplitude is 0.013 *volts*. The ripple also appears in the net power produced by the stack.

The PI controller for the heat exchanger achieves to regulate the air temperature ($T_{ca,in}$) to a value of 353.15 K at the cathode input, as indicated in the Fig. 6.

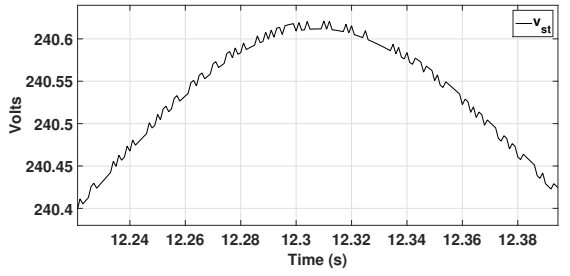

Fig. 5. Ripple over the voltage produced by the stack around the second 12.3.

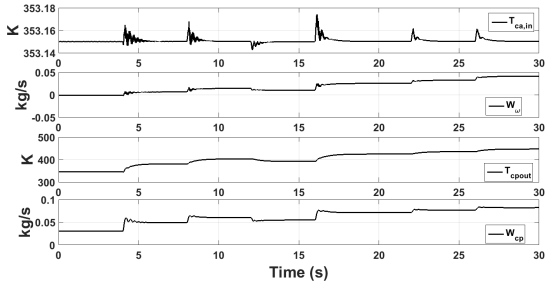

Fig. 6. Air temperature at the cathode inlet $T_(ca,in)$, mass flow of cooling water W_{ω}, air temperature at the compressor outlet $T_{cp,out}$, and y mass flow through the compressor W_{cp}, respectively.

The disturbances for this device are both variations in air temperature at the compressor output ($T_{cp,out}$) and variations in mass flow through the compressor (W_{cp}). Conveniently, the controller achieves to attenuate these disturbances efficiently avoiding damage to the polymer membrane.

It is true that the heat exchanger has a nonlinear model, but the fact of having dimensioned this device under demanding flow and temperature conditions allowed us to obtain design parameters that reduce the effects of nonlinearities. For this reason, the proportional and integral actions of its controller are sufficient to carry out the rejection of disturbances.

Observing the graph of the compressor output temperature ($T_{cp,out}$) it can be seen that it is not always greater than 353.15 K. In fact, when the current demanded by the load (I_{st}) is 110 *amperes*, $T_{cp,out}$ reaches no more than 344 K. In this situation it could be thought that the air needs to be heated, however the simulations indicate that neither the polymeric membrane nor the performance of the system deteriorate; like this, a conditional could be used in order to assign zero to both the flow of the cooling fluid in order to avoid that the heat exchanger be activated and the error of the PI in order to avoid the integral part modify its value.

The PI controller has a good performance reducing the pressures difference between the cathode and anode over the entire operation range (Fig. 7). In this control loop, Pukrushpan *et al.* (2004) used only a proportional action, so its performance lacked of unity gain. By including the integral action, a proper trajectory tracking is achieved.

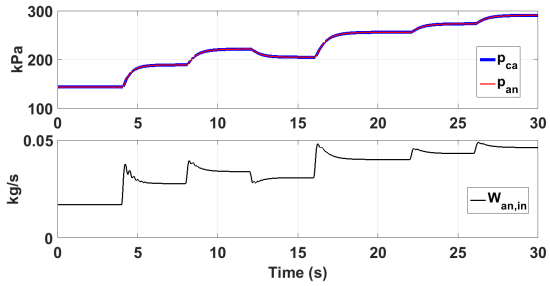

Fig. 7. Minimization of the pressures difference between the cathode p_{ca} and anode p_{an}.

The Fig. 8 shows the evolution of the state variables corresponding to the direct current electric motor. While the armature current has a maximum value of 41 amperes, the angular velocity of the motor reaches 10.514×10^3 rad/s just in the overshoot of the last transient period. Note also that the field current (i_f) has the same shape as the voltage (v_{st}) produced by the stack over the entire simulation time.

The efficiency with which the compressor makes the air flow depends on the pressure ratio (p_{sm}/p_{atm}) and the mass flow through it (W_{cp}) and its maximum value is 0.8, as indicated in the Fig. 9. The flow-pressure path following the load profile remains inside the operating limits described with blue lines in the Fig. 10. This means that, throughout the simulation, the compressor always operated inside its region of maximum efficiency, being $\eta_{cp} = 0.7$ the lowest value reached during the first transient period, as shown in the Fig. 11.

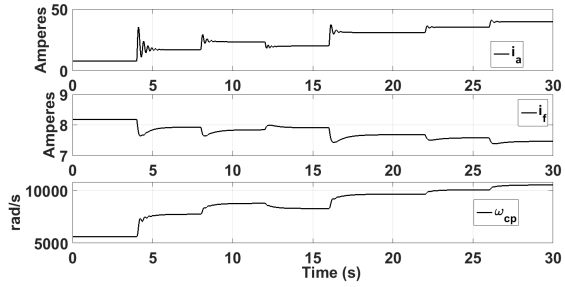

Fig. 8. Armature current i_a, field current i_f, and angular speed of the electric motor ω_{cp}, respectively.

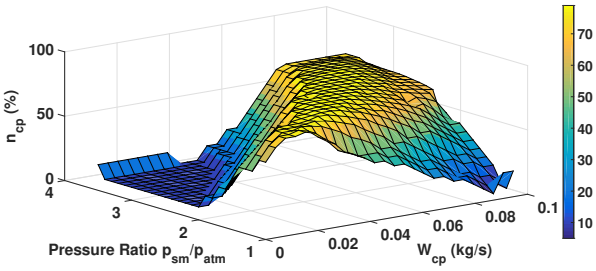

Fig. 9. Compressor efficiencies η_{cp} as a function of the pressure ratio p_{sm}/p_{atm} and the mass flow through the compressor W_{cp}.

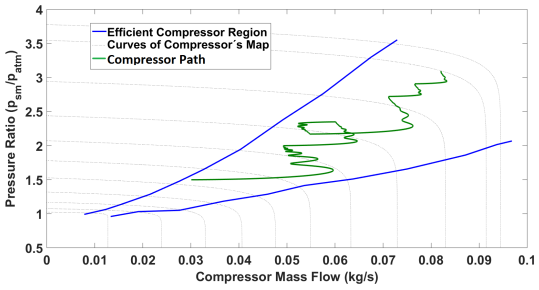

Fig. 10. Flow-Pressure path over compressors map.

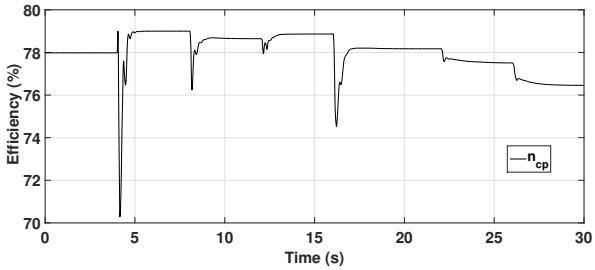

Fig. 11. Compressor efficiency η_{cp} throughout the simulation.

Finally, based on the ideal gas law, at constant temperature, pressure variations of the reactants will be caused by variations in the flow thereof. While moving between different polarization curves, the current-voltage path (Fig. 12) shows the pressure levels of the reactants. Furthermore, the value of voltage produced by each of the 381 fuel mono-cells is around 0.6 *volts*.

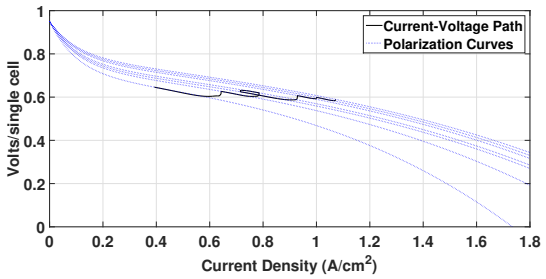

Fig. 12. Current-voltage path over the polarization curves.

Conclusions

The incorporation of equations describing the DC motor used to drive the compressor allowed to have a more realistic approach of both the power consumed by the electric motor and the net power delivered by the stack. Regarding its dynamics, it was possible to see that the overshoots in the power consumed by the motor causes a non-minimum phase response in the net power delivered by the stack.

For its part, the adaptive controller adequately regulated the oxygen excess ratio keeping it at a value of two throughout the operating range. Similarly, the hydrogen flow controller managed to equalize the pressure on both electrodes.

In addition, through a steady-state analysis, it was possible to design a heat exchanger capable of reducing the temperature of the air entering the cathode to the levels required by the fuel cell. The controller designed to regulate such temperature achieved acceptably attenuate disturbances introduced by changes in the flow and temperature of the fluid of interest.

After adding the auxiliary equipments, the fuel cell system is described with a total of thirteen differential equations: three belong to the cathode, two to the anode, two to the supply manifold, one to the return manifold, three to the direct current electric motor, and two further to the heat exchanger for the cathode.

Acknowledgements

The first author thanks the support to the Consejo Nacional de Ciencia y Tecnología (CONACYT) for the scholarship granted to study the Doctorate in Sciences in Electronic Engineering within the doctorate program of the National Center for Research and Technological Development.

Abbreviations

E	open circuit voltage, V
v_{act}	voltage due to activation losses, V
v_{ohm}	voltage due to Ohmic losses, V
m	mass , kg
n	number of mono-fuel cells
v_{st}	voltage produced by the stack, V
I_{st}	current demanded by the load, A
i	current, A
P_{net}	net power, kW
P_{st}	total power, kW
p	pressure, kPa
R	resistance, ω
L	inductance, mH
T	air temperature, K
W	mass flow, kg/s
	Greek symbols
λ_{O_2}	oxygen excess ratio
ω	cooling water
η	efficiencies
f	field
τ	torque, Nm
γ	relation of specific heats
	Subscripts
a	armature
ca	cathode
an	anode
in	input
out	output
cp	compressor
O_2	oxygen
N_2	nitrogen
H_2	hydrogen
cm	electric motor
sm	supplied manifold
rm	return manifold

References

Astorga Zaragoza, C.M., Alvarado Martínez, V.M., Zavala Ro, A., Mendez Ocaa, R.M. and Guerrero Ramírez G.V. (2008) Observer-based monitoring of heat exchangers. *ISA Transactions 47*, 15-24.

Åström, K.J. and Wittenmark, B. (2008). *Adaptive Control*. Second edition, 574 pages. Addison-

Wesley Mineola, New York.

Åström, K.J. and Hägglund, T., (1988). *PID Controllers: Theory, Design, and Tuning*. Second edition. Instrument Society of America, Lund, Sweden.

Bequette, B.W. (1998). *Process Dynamics, Modeling, Analysis, and Simulation*. Rensselaer Polytechnic Institute. Prentice Hall, Upper Saddle River, New Jersey.

Barelli, L., Bidini, G. and Ottaviano, A. (2011). Optimization of a PEMFC/battery pack power system for a bus application. *Applied Energy 27*, 777-784.

Cantero, C., López, G., Alvarado, V., Jimenez, R., Morales, J. and Coronado, E. (2017). Control structures evaluation for a salt extractive distillation pilot plant: Application to bio-ethanol dehydration. *Energies 10*, 1276.

de la Cruz, J., Romero, T. and Cano, U. (2018). *Nanostructured Materials for Next-Generation Energy Storage and Conversion*. Pp. 469-495. Springer, Berlin, Heidelberg.

de la Cruz J., Cano U. and Romero T. (2016). Simulation and *in situ* measurement of stress distribution in a polymer electrolyte membrane fuel cell stack. *Journal of Power Sources 329*, 273-280 .

Genyin, Y., Donglai, X., Weiyan, Q., Grace J.R. and Jim C.L. (2009) Modeling of fluidized bed membrane reactors for hydrogen production from steam methane reforming with Aspen Plus. *International Journal of Hydrogen Energy 34*, 4755-4762.

Gerard, M., Poirot Crouvezier, J.P, Hissel, D. and Pera M.C. (2012). Oxygen starvation analysis during air feeding faults in PEMFC. *International Journal of Hydrogen Energy 35*, 12295-12307.

Gómez, A., Zacarías, A., Venegas, M., Vargas, R.O., Carvajal, I. and Aguilar, J.R. (2018). Modeling and optimization of an Otto cycle using the ethanol-gasoline blend. *Revista Mexicana de Ingeniería Química 16*, 1065-1075.

Hosseinzadeh, E., Rokni, M., Rabbani A. and Mortensen, H.H. (2013.) Thermal and water management of low temperature proton exchange membrane fuel cell in fork-lift truck power system. *Applied Energy 104*, 434-444.

Hwang, J.J., Chen Y.J and Kuo, J.K. (2012). The study on the power management system in a fuel cell hybrid vehicle. *International Journal of Hydrogen Energy 37*, 4476 - 4489.

Ioan Dore, L. and Gianluca, Z., (2006). *Digital Control Systems: Design, Identification and Implementation*. Springer-Verlag London.

Khalil H.K. and Grizzle J. (1996). *Nonlinear Systems*. Prentice hall New Jersey.

Ljung, L. (1999). *System Identification: Theory for the User*. Upper Saddle River, Prentice Hall, New Jersey.

Luyben, W.L. (2002). *Plantwide Dynamic Simulators in Chemical Processing and Control*. Lehigh University. Bethlehem, Pennsylvania. Marcel Dekker.

Maya Yescas, R., Salazar Sotelo, D., Mariaca Domínguez, E., Rodríguez Salomón, S. and García Moreno, L. M. (2006). Fluidized-bed catalytic cracking units emulation in pilot plant. *Revista Mexicana de Ingeniería Química 5*, 97-103.

Nikiforow, K., Pennanen, J., Ihonen, J., Uski, S. and Koski P. (2018). Power ramp rate capabilities of a 5 kW proton exchange membrane fuel cell system with discrete ejector control. *Journal of Power Sources 381*, 30-37.

Ogata K., (2002). *Ingeniería de Control Moderna*. Prentice Hall, Nueva York.

Pérez Rodríguez, P., Martínez Amador, S., Valdez Aguilar, L., Benavides Mendoza, A., Rodríguez de la Garza, J., and Ovando Medina, V. (2018). design and evaluation of a sequential bioelectrochemical system for municipal wastewater treatment and voltage generation. *Revista Mexicana De Ingeniería Química 17*, 145-154.

Pukrushpan, J.T., Stefanopoulou, A.G. and Peng, A.G. (2004). *Control of Fuel Cell Power Systems: Principles, Modeling, Analysis and Feedback Design*. Springer-Verlag London.

Pukrushpan, J.T., (2003). *Modeling and Control of Fuel Cell Systems and Fuel Processors*. Ann Arbor, Michigan. Springer.

Pukrushpan, J.T., Stefanopoulou, A.G. and Peng, H. (2002). Modeling and control for PEM fuel cells stack system. *Proceedings of the American Control Conference, IEEE 4*, 3117-3122.

Rabbani, A., Rokni, M., Hosseinzadeh, E. and Hilleke Mortensen, H. (2014). The start-up analysis of a PEM fuel cell system in vehicles. *International Journal of Green Energy Volume 11*, 91-111.

Rubio, J.de J., Figueroa, M., Pérez Cruz, J.H., and Rumbo, J.Y. (2012). Control para estabilizar y atenuar las perturbaciones en un péndulo invertido rotatorio. *Revista Mexicana de Física E 58*, 107-112.

Rumbo Morales, J.Y., Lopez Lopez, G., Alvarado, V.M., Valdez Martinez, J.S., Sorcia Vázquez, F.D.J. and Brizuela Mendoza, J.A. (2018). Simulation and control of a pressure swing adsorption process to dehydrate ethanol. *Revista Mexicana de Ingeniería Química 17*, 1051-1081.

Schefflan, R. (2011). *Teach Yourself the Basics of Aspen Plus*. Chemical Engineering and Materials Science Department. AIChE, John Wiley and Sons, Hoboken, New Jersey.

Sveshnikova, A., Di Marcoberardino, G., Pirrone, C., Bischi A., Gianluca, V., Ustinova, A. and Campanari, S. (2017). The impact of humidification temperature on a 1 kW proton exchange membrane fuel cell stack. *Energy Procedia Volume 142*, 1661-1667.

Téllez Méndez, N., Gamboa Sánchez, S.A. Paniagua Solar, L.A. and Guerrero Castellanos, J.F. (2018). Síntesis y evaluación del electrocatalizador $Pt/Al_2O_3/c$ para su futura aplicación en celdas de combutible de bio-etanol directo. *Revista Mexicana de Ingeniería Química 17*, 477-483.

Wu, H.W. (2016). A review of recent development: Transport and performance modeling of PEM fuel cells. *Applied Energy 165*, 81-106.

Zhai S.,Sun, P., Chen, F., Zhou, S. and Zhang, Ch. (2010). Collaborative simulation for dynamical PEMFC power systems. *Hydrogen Energy 35*, 8772-8781.